Contribution of Human Manganese Superoxide Dismutase Tyrosine 34 to Structure and Catalysis†

J. Jefferson P. Perry,*,‡,§ Amy S. Hearn,|| Diane E. Cabelli,⊥ Harry S. Nick,|| John A. Tainer,‡,# and David N. Silverman*,+

Department of Molecular Biology, The Scripps Research Institute, La Jolla, California 92037, School of Biotechnology, Amrita University, Kollam, Kerala 690525, India, Life Sciences Division, Department of Molecular Biology, Lawrence Berkeley National Laboratory, Berkeley, California 94720, Department of Chemistry, Brookhaven National Laboratory, Upton, New York 11973, Department of Neuroscience, University of Florida, Gainesville, Florida 32510, and Department of Pharmacology, University of Florida, Gainesville, Florida 32610

Received December 20, 2008; Revised Manuscript Received February 26, 2009

ABSTRACT: Superoxide dismutase (SOD) enzymes are critical in controlling levels of reactive oxygen species (ROS) that are linked to aging, cancer, and neurodegenerative disease. Superoxide ($O_2^{\bullet-}$) produced during respiration is removed by the product of the SOD2 gene, the homotetrameric manganese superoxide dismutase (MnSOD). Here, we examine the structural and catalytic roles of the highly conserved active-site residue Tyr34, based upon structure−function studies of MnSOD enzymes with mutations at this site. Substitution of Tyr34 with five different amino acids retained the active-site protein structure and assembly but caused a substantial decrease in the catalytic rate constant for the reduction of superoxide. The rate constant for formation of the product inhibition complex also decreases but to a much lesser extent, resulting in a net increase in the level of product inhibited form of the mutant enzymes. Comparisons of crystal structures and catalytic rates also suggest that one mutation, Y34V, interrupts the hydrogen-bonded network, which is associated with a rapid dissociation of the product-inhibited complex. Notably, with three of the Tyr34 mutants, we also observe an intermediate in catalysis, which has not been reported previously. Thus, these mutants establish a means of trapping a catalytic intermediate that promises to help elucidate the mechanism of catalysis.

The superoxide dismutases are found in prokaryotes, archaea, and eukaryotes, where they catalyze the disproportionation of the superoxide radical anion $O_2^{\bullet-}$ in cellular processes detoxifying reactive oxygen species (*1*). The mechanism by which all superoxide dismutases carry out the catalytic removal of superoxide involves an oxidation−reduction cycle, as shown in the reactions below.

$$M^{(n+1)} + O_2^{\bullet-} \rightarrow M^{(n)} + O_2$$

$$M^{(n)} + O_2^{\bullet-} + 2H^+ \rightarrow M^{(n+1)} + H_2O_2$$

In humans, three SOD (*1*) enzymes exist. SOD1 is a cytoplasmic Cu,Zn SOD, SOD2 a mitochondrial MnSOD, and SOD3 an extracellular Cu,Zn SOD. These SOD enzymes are critical in controlling levels of reactive oxygen species (ROS) that are linked to aging, cancer, and neurodegenerative disease (*2*). Structure−activity relationships for this class of enzymes need to be understood and distinguished, as their disease phenotypes likely occur through different mechanisms. SOD1 is a Cu,Zn dimeric enzyme with a β-barrel fold (*3*) with an active-site channel containing a site for superoxide substrate and hydrogen peroxide product binding (*4, 5*) adjacent to the activity important Arg143 side chain (*6*). The structure of human Cu,Zn SOD resembles that of bacterial Cu,Zn SOD except the dimer contact is on the opposite surface (*7, 8*). For the human Cu,Zn SOD, dimer- and framework-destabilizing mutations in SOD1 give rise to amyotrophic lateral sclerosis (ALS), also known as Lou Gehrig's disease (*9*−*11*), a progressive neurological disease caused by the degeneration of motor neurons. Additionally, the Zn site of Cu,Zn SOD likely contributes to ALS (*12, 13*), suggesting that the presence of a bivalent metal ion site contributes to degenerative disease. MnSOD instead contains a single metal ion site, and destabilizing mutations in MnSOD are not reported to cause severe disorders (*14, 15*); however, a couple of polymorphisms are indicated in disease phenotypes (*16*−*20*). Moreover, MnSOD has a critical function in maintaining the integrity of mitochondrial enzymes that are susceptible to direct inactivation by superoxide (*21*).

† This work was supported by National Institutes of Health Grant GM54903 to D.N.S.

* To whom correspondence should be addressed. D.N.S.: phone, (352) 392-3556; fax, (352) 392-9696; e-mail, silvrmn@ufl.edu. J.J.P.P.: phone, (858) 784-2284; fax, (858) 784-2277; e-mail, jjperry@scripps.edu.

‡ The Scripps Research Institute.

§ Amrita University.

|| Department of Neuroscience, University of Florida.

⊥ Brookhaven National Laboratory.

Lawrence Berkeley National Laboratory.

+ Department of Pharmacology, University of Florida.

[1] Abbreviations: SOD, superoxide dismutase; ROS, reactive oxygen species; ALS, amyotrophic lateral sclerosis; rmsd, root-mean-square deviation; Taps, 3-{[tris(hydroxymethyl)methyl]amino}propanesulfonic acid; Mops, 3-(*N*-morpholino)propanesulfonic acid.

10.1021/bi8023288 CCC: $40.75
Published on Web 03/05/2009

MnSOD is a homotetrameric protein controlling the detoxification of $O_2^{\bullet-}$ produced as a minor side product of respiration in the mitochondria. Besides its intrinsic importance, this tetrameric MnSOD provides an important comparative enzyme of medical relevance as the smaller dimeric Cu,Zn SOD is rapidly cleared from human serum and mutants designed to form tetramers and larger assemblies result in structural distortions (*22*). The manganese site furthermore differs from the Cu,Zn SOD active site by being in a trigonal bipyramidal geometry with four ligands from the protein and a fifth solvent ligand (*14*). The bound solvent ligand is a hydroxide for the oxidized enzyme Mn^{3+}SOD near physiologic pH; this is believed to be the acceptor for proton transfer upon reduction of the enzyme (*23, 24*). The structure of MnSOD resembles that of bacterial FeSOD; however, details of their active-site chemistries are different (*25*). Catalysis by MnSOD is subject to a substantial and reversible product inhibition by peroxide, arising from the oxidative addition of superoxide to Mn^{2+}SOD (*26*). This is different from the deactivation of the active site of FeSOD through Fenton chemistry (*27*). The kinetics of catalysis by MnSOD is consistent with the formation of a reversible, dead-end complex, and although the structure of this complex has not been observed, spectroscopic and computational considerations seem to favor a side-on peroxo complex of the metal (*26, 28*). The complex was first observed as a rapidly emerging zero-order phase of catalysis (*26, 29*).

The active-site cavity of MnSOD is characterized by a hydrogen-bonded network extending from the aqueous ligand of the metal and comprising the side chains of several residues, including Tyr166 emanating from an adjacent subunit (*14*). Included in this network is the highly conserved residue Tyr34 (*30*), the side chain of which participates in hydrogen bonding with both Gln143 and an adjacent water molecule (*14, 31*). Tyr34 plays a key role in the hydrogen bonding network, as nitration of the active-site residue Tyr34 causes nearly complete inhibition of catalysis (*32*). However, the precise role of this network in catalysis is not determined experimentally, yet computational analyses support a role for proton transfer from Tyr34 providing one of the two protons to form H_2O_2 in catalysis (*28*). Replacement of Tyr34 in MnSOD has rather modest effects on the k_{cat}/K_m of catalysis (*33, 34*); however, k_{cat} is decreased ~10-fold (*33*). The structure of human Y34F MnSOD has been determined (*33*), and the role of Tyr34 in the spectral and catalytic properties of human and bacterial MnSOD has been examined in several studies of Y34F MnSOD (*33*−*37*). The ionization of Tyr34 with a pK_a near 9.5 is the source of spectroscopic changes in Mn^{3+}SOD (*25, 38*) and probably is responsible for the decrease in catalytic activity as the pH increases beyond 9 (*34*). There is a role of Tyr34 in avoiding product inhibition; the replacement of Tyr34 with Phe (Y34F) resulted in a level of product inhibition greater by ~80-fold than that of the wild type (*35*). The rate of dissociation of hydrogen peroxide from product-inhibited enzyme is decreased only 2-fold in Y34F (*33*) and is unchanged in a form of human MnSOD in which all tyrosine residues were replaced with 3-fluorotyrosine (*39*).

To address key questions regarding the role of residue 34 in MnSOD activity, we report here comprehensive mutational analyses of residue 34, which describe the effect of mutations on both the crystal structure and catalysis. The data show that substitution of Tyr34 with five different amino acids is associated with a substantial decrease in the rate constant for the reduction of superoxide in the catalytic cycle. The rate of formation of the product-inhibited complex is much less reduced however, which results in a net increase in the product-inhibited form of these mutant enzymes. Comparisons of crystal structures and rates of catalysis also indicate that interruption of the hydrogen-bonded network in the active site results in a significantly increased rate of dissociation of the product from the inhibited complex. Furthermore, an intermediate in catalysis that has not been reported previously is observed in three residue 34 mutants, which may eventually help elucidate the detailed molecular mechanism of catalysis.

EXPERIMENTAL PROCEDURES

Crystallography. Orthorhombic crystals of Y34H and Y34N human MnSOD were grown by vapor diffusion from solutions consisting of 26 and 24 mg/mL protein, respectively, buffered in 25 mM potassium phosphate (pH 7.8) and 22% poly(ethylene glycol) (PEG) 2000 monomethyl ether. Large hexagonal crystals of Y34V and Y34A human MnSOD were grown from 22 and 18 mg/mL protein, respectively, buffered in 2.5 M ammonium sulfate and 100 mM imidazole/malate buffer (pH 7.5). Single crystals were used for data collection and were cryoprotected with 20% ethylene glycol in the well solution, before being frozen in a stream of liquid nitrogen. The Y34H, -N, and -V MnSOD data sets were collected at the Stanford Synchotron Radiation Laboratory (SSRL) on beamline 9-1, and the Y34A mutant data set was collected at the Advanced Light Source (ALS), Lawrence Berkeley National Laboratory, on beamline 8.3.1. The collected data sets were indexed and merged with DENZO and scaled with Scalepack (*40*). Phases were determined by molecular replacement from the wild-type structure using AMoRe (*41*). The structures were refined with several cycles of rigid body and restrained refinement, using Crystallography and NMR Systems, version 1.1 (CNS) (*42*). Final refinement steps for the higher-resolution Y34N mutant MnSOD were completed using SHELX (*43*). Models were rebuilt to σA-weighted $2F_o - F_c$ and $F_o - F_c$ maps using Xfit (*41*). The data collection and refinement statistics of these four mutants are listed in Table 1. Atomic coordinates have been deposited in the Protein Data Bank as entries 1ZSP for Y34A, 1ZTE for Y34H, 2P4K for Y34N, and 1ZUQ for Y34V.

Pulse Radiolysis. These experiments were carried out at the Brookhaven National Laboratory using a 2 MeV van de Graaff accelerator. UV−visible spectra were recorded using a Cary 210 spectrophotometer with a path length of 2.0 or 6.1 cm. Solutions contained enzyme and 30 mM sodium formate as a hydroxyl radical scavenger (*44*), 50 μM EDTA, and 2 mM buffer (Mops at pH 6.5−7.3, Taps at pH 7.4−9.3, and Ches at pH 9.4−10.5). Reported rate constants were obtained using the manganese concentration from atomic absorption spectrometry rather than the total protein concentration, with all manganese assumed to be at the active site of MnSOD.

Superoxide radicals were generated by exposing air-saturated solutions to an electron pulse. In our solutions, the primary radicals created by the pulse are converted to

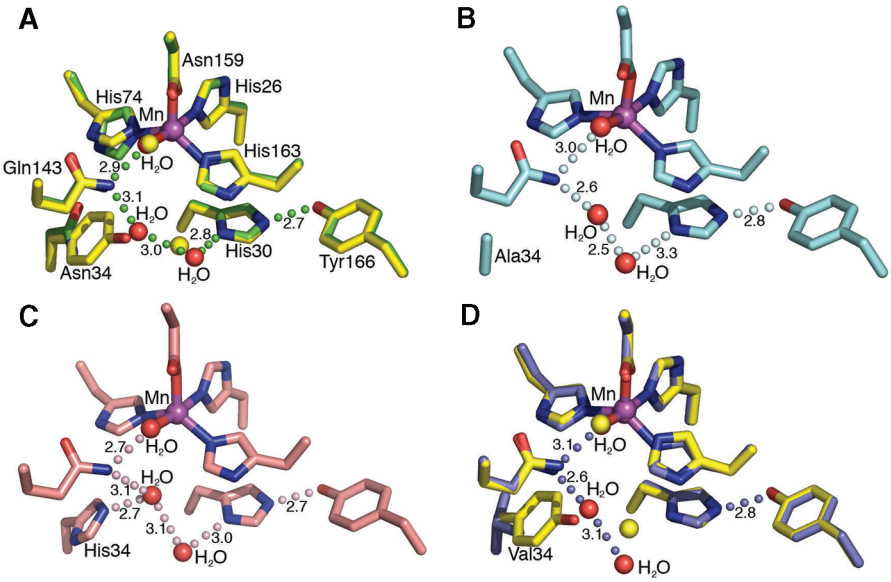

FIGURE 1: MnSOD active-site structure and residue 34 mutations. (A) Superimposition of the active-site side chains, manganese ion, and ordered solvent molecules of human wild-type MnSOD (yellow) and Y34N (green). Y34N waters are colored red (wild-type waters colored yellow); green spheres depict the Y34N hydrogen bond relay, and the bond distances, in angstroms, are annotated. (B) Active site of the Y34A crystal structure, with the hydrogen bonding relay maintained and colored pale cyan. (C) Active site of the Y34H crystal structure, with the hydrogen bonding relay and distances, in angstroms, annotated. (D) Superimposition of the active-site chains of human wild-type MnSOD (yellow) and Y34V (blue). Replacement of Tyr34 with Val interrupts the hydrogen bond network. The Y34V waters are colored red (wild-type waters colored yellow); and the hydrogen bond relay of Y34V MnSOD is depicted with blue spheres, and bond distances, in angstroms, are annotated.

Table 1: Crystallographic Data and Refinement Statistics

	Y34A	Y34H	Y34N	Y34V
space group	$P6_122$	$P2_12_12_1$	$P2_12_12_1$	$P6_122$
unit cell dimensions (Å)				
a	79.52	73.67	73.56	79.63
b	79.52	77.84	73.56	79.63
c	242.99	136.22	136.10	241.64
wavelength (Å)	1.06	0.95	1.03	0.95
resolution (Å)	50−1.9	37.4−1.85	39.2−1.48	39.7−2.0
no. of theoretical/observed reflections (last shell)	34791/31760 (5658)	67566/61782 (8683)	130469/126423 (20100)	31662/30942 (4984)
% completeness (last shell)	91.2 (94.6)	91.4 (82.9)	96.9 (93.4)	97.6 (96.8)
$\langle I/\sigma I \rangle$ (last shell)	48.9 (11.5)	15.2 (3.0)	26.9 (5.0)	28.6 (5.4)
R_{merge} (last shell)	5.0 (15.2)	8.6 (30.6)	6.0 (29.9)	5.5 (22.6)
model statistics				
R_{free}	28.6	24.5	22.2	27.4
R_{work}	23.9	20.6	16.0	23.5
rmsd for bond lengths (Å)	0.005	0.005	0.004	0.005
rmsd for bond angles (deg)	1.2	1.2	1.2	1.2
rmsd from WT MnSOD, subunits a, b, c, and d	0.25, 0.2	0.27, 0.33, 0.21, 0.26	0.26, 0.34, 0.23,0.25	0.2, 0.25

superoxide by a number of scavenging reactions listed by Schwarz (*44*). In these experiments, superoxide formation is more than 90% complete within the first microsecond after the pulse. Catalysis was measured from the changes in absorption of superoxide (*45*) and of the enzyme itself (*46, 47*). Repeated pulses of electrons using the same enzyme sample gave identical catalytic rates; the radiolysis itself did not alter the catalysis. The data were analyzed and rate constants obtained by fits to changes in the spectra of enzyme and superoxide after generation of superoxide by pulse radiolysis. Analysis was performed using the BNL Pulse Radiolysis Program as described previously (*46, 47*). Identical values were obtained by the enzyme kinetics curve fitting package of Enzfitter (Biosoft).

RESULTS

Crystal Structures. To examine the role of Tyr34 in MnSOD activity, we determined and refined X-ray crystal structures that define the effect of mutations on the detailed active-site structural chemistry, as a structural framework for interpretation of their catalytic features. The Tyr34 mutants Y34A, -H, -N, and -V MnSOD structurally determined in these studies demonstrate that their subunit fold and tetrameric assemblies closely resemble those of the wild-type structure (*14*), supporting the use of these mutants in mechanistic analyses. The root-mean-square deviations (rmsd) for superimposition of all 198 Cα atoms for each mutant structure onto the wild type are listed in Table 1; the largest rmsd in the four mutants is only 0.34 Å from the wild-type structure, for one of the Y34N subunit structures in the asymmetric unit. These four mutant protein structures also exhibit minimal changes to the position and orientation of the active-site residues, including the manganese ion ligands (Figure 1).

In the wild-type enzyme, a hydrogen bonding network involving Tyr34 extends from the metal to Tyr166 (Mn-H_2O-

Table 2: Kinetic Constants for the Dismutation of Superoxide by MnSOD and Mutants[a]

enzyme	k_1 (nM^{-1} s^{-1})	k_2 (nM^{-1} s^{-1})	k_3 (nM^{-1} s^{-1})	k_3' (s^{-1})	k_4 (s^{-1})
wild-type	1.5	1.5	1.1	−	120
Y34A	0.25	<0.02	0.38	1600	330
Y34N	0.14	<0.02	0.15	850	200
Y34H	0.07	<0.02	0.04	250	61
Y34V	0.15	<0.02	0.15	−	1000
Y34F[b]	0.55	<0.02	0.46	−	52

[a] Conditions as described for Figure 2. The pH was 8.2 and the temperature 25 °C. Standard errors in these rate constants were in the range of 3−5%. [b] From ref *35*.

Gln143-Tyr34-H_2O-His30-Tyr166), where Tyr166 emanates from an adjacent subunit. All the mutations tested at position 34 alter this network (Table 1). In each of the four mutant structures, Y34A, -N, -H, and -V, the replacement of Tyr34 with a smaller side chain creates a cavity that is filled by an additional water molecule (Figure 1). In three of the structures (Y34A, -N, and -H), this additional water molecule maintains the hydrogen bonding network (Figure 1A−C). This water molecule forms hydrogen bonds to the Gln143 NE2 atom and to the water hydrogen bonded to the His30 ND1 atom in all four subunits of Y34H, two of the four subunits of Y34N, and one of the two subunits of Y34A within the crystallographic asymmetric unit. In the Y34H structure, this additional water molecule also forms a hydrogen bond to the His34 NE2 atom. Such additional water molecules have often been observed in cases of replacements with amino acids with a smaller volume in human MnSOD (*35, 46, 48, 49*).

The structure with the mutation of Tyr34 to nonpolar Val (Y34V MnSOD) differs from the other mutant structures in the disruption of the hydrogen bond relay observed in the crystal structure of the wild-type enzyme (Figure 1D). This disruption of the hydrogen bond relay is however similar to some other active-site mutations of human MnSOD (*33, 48, 50*). In Y34V MnSOD, the hydrogen bond to the Gln143 NE2 atom by the additional water molecule is maintained, but in both structures in the asymmetric unit, this water molecule is observed to form a hydrogen bond to a water molecule on the edge of the active-site cavity instead of the His30 ND1 atom (Figure 1D). An additional water was not observed in the crystal structure of Y34F MnSOD at 1.9 Å resolution (*33*); however, at a higher resolution of 1.5 Å, such a water molecule was observed in Y34F human MnSOD in which all remaining tyrosine residues were replaced with 3-fluorotyrosine (*31*).

Catalysis. To examine the effect of Tyr34 mutations on catalysis, we observed the absorbance spectrum of MnSOD and its mutants after the generation of superoxide by pulse radiolysis. Data were analyzed in terms of the model of catalysis shown in eqs 1−4 (*29*) and based on pulse radiolysis studies of MnSOD from *Bacillus stearothermophilus*. The MnSOD catalysis comprises two stages of an oxidation−reduction cycle with proton transfer ultimately from solution to final product H_2O_2. The redox cycle of catalysis is represented as two irreversible steps, reactions 1 and 2, justified in part by the favorable equilibrium constants associated with these processes. Reactions 3 and 4 are the formation and dissociation of an inhibited complex $Mn^{3+}(O_2^{2-})SOD$, respectively; the structure of this inhibited complex is not known, but data suggest it is a peroxo complex of the metal formed by an oxidative addition of superoxide to $Mn^{2+}(H_2O)SOD$ (*26*). These specific rate constants k_1-k_4 were obtained from rates of change in absorbance of MnSOD and superoxide as described previously (*35*). The results for Tyr34 mutants reveal the importance of this site for catalysis (Table 2).

$$Mn^{3+}(OH^-)SOD + O_2^{\bullet -} + H^+ \xrightarrow{k_1} Mn^{2+}(H_2O)SOD + O_2 \quad (1)$$

$$Mn^{2+}(H_2O)SOD + O_2^{\bullet -} + H^+ \xrightarrow{k_2} Mn^{3+}(OH^-)SOD + H_2O_2 \quad (2)$$

$$Mn^{2+}(H_2O)SOD + O_2^{\bullet -} \xrightarrow{k_3} Mn^{3+}(O_2^{2-})SOD + H_2O \quad (3)$$

$$Mn^{3+}(O_2^{2-})SOD + H^+ + H_2O \xrightarrow{k_4} Mn^{3+}(OH^-)SOD + H_2O_2 \quad (4)$$

Table 2 lists rate constants for reactions of eqs 1−4 for five site-specific mutants of human MnSOD studied here, including the previously reported Y34F mutant (*33, 35*). All of the examined Tyr34 mutants show substantial decreases in the second-order rate constants, k_1-k_3, in the catalytic cycle; however, k_2 is decreased to a much larger extent. These constants can be viewed in terms of a gating ratio k_2/k_3 that determines the flux through the catalytic and inhibition pathways. When this gating ratio is large, the pathway favors catalysis by eqs 1 and 2, and when the ratio is less than unity, the pathway favors formation of the inhibited complex. For human wild-type MnSOD, the gating ratio k_2/k_3 is near unity, but for the mutants of Table 2, this ratio is considerably less than unity. The rate constants k_4 describing the dissociation of the product-inhibited complex were also affected by these replacements (Table 2). They were greater for Y34V, Y34A, and Y34N compared with that of wild-type MnSOD and smaller for Y34F and Y34H.

For wild-type Mn^{2+}SOD and mutants Y34F and Y34V Mn^{2+}SOD (Table 2), the increase in absorbance at 420 nm following introduction of superoxide by pulse radiolysis can be well fit by a single exponential with rate constant k_3 describing the emergence of the product-inhibited form (as in eq 3; typical data are presented in Figure S1 of the Supporting Information). This has been the usual observation for many other mutants of human MnSOD studied by pulse radiolysis (*35, 36*). We report here the new observation that for mutants Y34A, Y34N, and Y34H there was an intermediate apparent in the catalysis. This is evident in the biphasic increase in the 420 nm absorption measured less than 2 ms after generation of $O_2^{\bullet -}$ by pulse radiolysis (Figure 2A). For these mutants (Y34A, Y34N, and Y34H), we observed an increase at 420 nm that is not described by a single exponential but is best fit by the sum of two exponentials with rate constants k_3 and k_3' given in Table 2. Here k_3' represents the formation of an intermediate approaching a

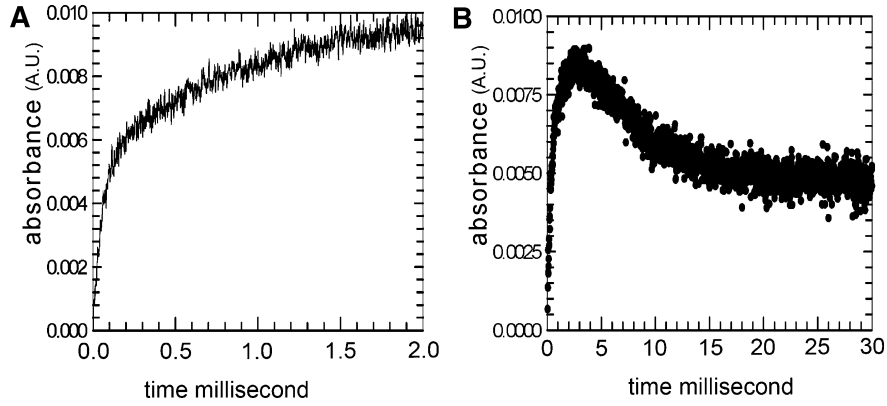

FIGURE 2: MnSOD activity and effect of the Y34N mutation. (A) The increase in absorbance (absorbance units) at 420 nm of 120 μM Y34N MnSOD in the 2 ms after pulse radiolysis generated initial superoxide concentrations of 5 mM. (B) Same experiment at longer times. Solutions contained 30 mM formate, 50 μM EDTA, and 2 mM Taps (pH 8.2). The enzyme had been reduced prior to the experiment with 130 μM H_2O_2. The data are fit to eqs 1−4, resulting in the entries in Table 2.

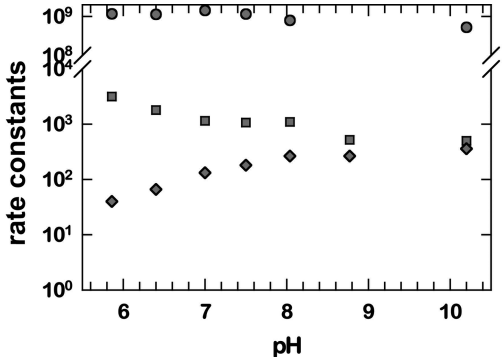

FIGURE 3: pH profiles for rate constants k_1 (M^{-1} s^{-1}) (circles), k_3' (s^{-1}) (squares), and k_4 (s^{-1}) (diamonds) in catalysis by Y34N MnSOD. Experiments used no added NaCl, matching the lowest ionic strength in Figure 4. Experiments were conducted in 10 mM formate, 10 mM phosphate, and 25 μM EDTA at 25 °C. The measurements were taken at pH 7.0, a pH somewhat lower than that used in the other studies.

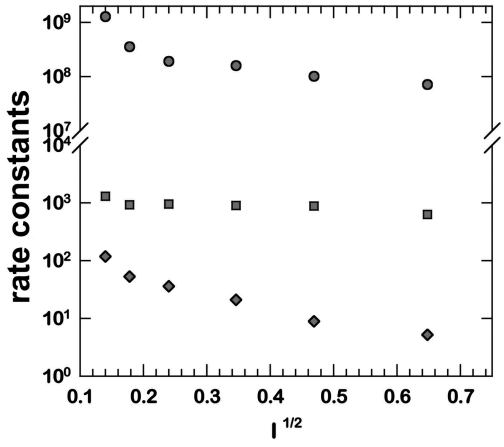

FIGURE 4: Ionic strength (I) profiles for the rate constants k_1 (M^{-1} s^{-1}) (circles), k_3' (s^{-1}) (squares), and k_4 (s^{-1}) (diamonds) in catalysis by Y34N MnSOD. Conditions are listed in the legend of Figure 3, with the ionic strength adjusted by addition of NaCl.

maximum at 420 nm that appears fully formed by 2 ms (Figure 2A,B).

Three well-defined rate constants of the mechanism of eqs 1−4 are further investigated for Y34N in the pH and ionic strength profiles of Figures 3 and 4. Here it appears that k_1 is independent of pH in the range measured; however, k_3' and k_4 show a variation below pH 8 that is complex and not

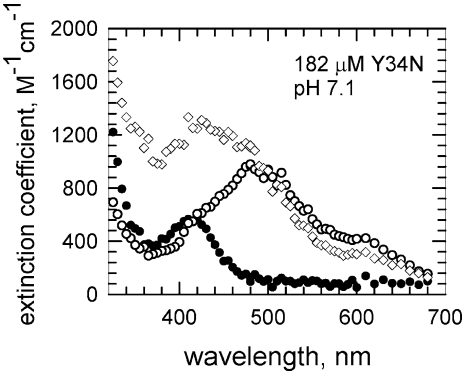

FIGURE 5: Molar extinction coefficients (M^{-1} cm^{-1}) observed after pulse radiolysis of a solution of Y34N MnSOD (182 μM) at pH 7.1 pre-reduced with H_2O_2: (○) spectrum of Mn^{3+}(OH)SOD obtained by extrapolating to long times in Figure 2A, (●) spectrum of the product-inhibited complex obtained by extrapolating the initial increase (t = 0.2 ms) as in Figure 2A, and (◇) spectrum of a newly detected intermediate obtained by extrapolating the second kinetic process at times near 2 ms as in Figure 2B. Solutions contained 30 mM formate, 50 μM EDTA, and 2 mM Mops.

fit to a single ionization. One possible explanation for almost no pH dependence in k_1 (Figure 3) is that the protons involved emanate from groups with values of pK_a outside the pH range of these studies. The variation with ionic strength shows variations of k_1 and k_4, but most notably, the rate constant k_3' is independent of changes in ionic strength (Figure 4).

When the data for Y34N in Figure 2A were separated into their two exponential increases and the molar extinction coefficients near 2 ms were plotted as a function of wavelength, the resulting spectrum showed an absorption maximum at 420−440 nm with a molar extinction coefficient near 1300 M^{-1} cm^{-1} (Figure 5). The maximal absorption of the initial, rapid increase (<0.2 ms) when plotted as a function of wavelength is the spectrum of the inhibited complex. This has a maximum at 420 nm with a molar extinction coefficient of 600 M^{-1} cm^{-1} (Figure 5), consistent with previous reports of the product-inhibited complex (*26, 46*). At long times near 30 ms, the enzyme species equilibrate (Figure 2B) to a maximum at 480 nm and a molar extinction coefficient near 900 M^{-1} cm^{-1}, which is consistent with Mn^{3+}(OH)SOD (*26*). These plots were similar for the other variants that showed an intermediate, Y34A and Y34H. The plot for Y34A is shown in Figure S2 of the Supporting Information.

DISCUSSION

To investigate the function of residue 34 of human MnSOD in catalysis and inhibition, we replaced the highly conserved active-site residue Tyr34 with selected amino acids. Among the Tyr34 variants examined, only wild-type MnSOD maintains the most efficient catalysis (Table 2). Each of the mutants caused a decrease in rate constants k_1 and k_2 describing the catalytic cycle, and in k_3 which describes the formation of the product-inhibited complex (eqs 1−4). However, k_2 was more greatly affected with values of rate constants that were too low to measure accurately. This observation helps to explain the increased level of product inhibition in Y34F MnSOD (*33*) and other mutants at position 34 compared with that of the wild type; this is due to the greatly decreased rate constant k_2 for the catalytic reduction of $O_2^{\bullet-}$ to hydrogen peroxide, rather than an increased rate through the pathway described by k_3 leading directly to the inhibited state.

The large decreases in k_2 observed for the mutants of Table 2 are probably not due to changes in midpoint potential at the active site; the redox potential of Y34F MnSOD is not significantly different from that of the wild type (*51*). Rather, k_2 likely describes Tyr34 as a source of one of the two protons that is transferred to product H_2O_2, a scheme that is supported by experimental and computational evidence (*28*). This explains why, relative to the large decreases in k_2, there are decreases that are much smaller magnitude in k_1 and k_3, steps that do not involve rate-contributing proton transfer (*46*). The enzyme has a fast protonation pathway described by k_2 of eq 2 and a slower protonation pathway described by k_4. The data suggest that Tyr34 is involved in the fast pathway because k_2 is greatly reduced in mutants at this site.

The values of the rate constant for the dissociation of the inhibited complex, k_4, appeared to be greater for some mutants and smaller for others compared with that of wild-type MnSOD (Table 2). This rate constant is dependent on proton transfer as a rate contributing step (*46*). The mutant with the largest value of k_4 is Y34V MnSOD; this is the only mutant of those studied in Table 2 for which no hydrogen bonded network is observed. Hence, we suggest that the proton transfer involved in k_4 does not involve this hydrogen bonded network. This result is consistent with the conclusion made using MnSOD containing 3-fluorotyrosine (*31*) that Tyr34 is not involved in proton transfer to the product-inhibited complex.

Besides the well-studied, reversible product-inhibited complex, this work shows evidence of a second intermediate formed with rate constant k_3' in catalysis by Y34A, Y34N, and Y34H that appears in the initial 2 ms of catalysis (Figure 2A). (The first intermediate is the product-inhibited complex.) By separation of the kinetic data into their individual exponential increases, we have an absorption spectrum of this intermediate showing a maximum at 420−440 nm and a molar extinction coefficient of 1300 M^{-1} cm^{-1} (Figure 5). Since this intermediate is observed in mutants for which Tyr34 is replaced, it is not due to formation of a tyrosine radical, nor are its absorption characteristics consistent with a tryptophan radical.

The variation of selected rate constants with pH in Figure 3 shows that k_1 is independent of pH in the range studied. This means that the rapid electron transfer of eq 1 occurs without the influence of a nearby ionizable group such as Tyr34 or His30. Any proton transfer within the steps described by k_1 is not influenced by groups having a pK_a in the range of 6−10. This is not the case for k_3' and k_4, both of which show a variation with pH below pH ∼8. In each case, this variation with pH is not fit by a single ionization; that is, the variation of the rate constants depends on the ionization states of enzyme species in a more complex manner. The variation of these rate constants with the ionic strength of the solution (Figure 4) offers further information. Here, k_1 and k_4 vary with ionic strength, consistent with the mechanism of eqs 1 and 4 which show changes in electrostatic charge associated with formation of products O_2 and H_2O_2 in these steps.

However, the rate constant k_3' does not vary with ionic strength. This suggests that an isomerization or transition not involving a change in electrostatic charge is involved, such as addition of a solvent molecule to the ligand field of the metal. Perhaps the second intermediate may represent an enzyme species with a solvent molecule as a sixth ligand of the metal. Support for a sixth ligand comes from both the cryo-crystal structure of *E. coli* MnSOD containing a six-coordinate, distorted-octahedral active site (*52*) and the six-coordinate manganese active site observed in the azide complex of archeal MnSOD (*53*). Moreover, one proposed mechanism for MnSOD catalysis is the "5-6-5 mechanism", where in the resting state the metal ion is five-coordinated while upon anion binding it forms a six-coordinate state (*53*). The steps associated with k_3' may involve two binding sites, the first of which represents a binding site not on the metal and the second a stable metal-bound species. This could involve, for example, displacement of a metal-bound peroxy intermediate or displacement of the ligand Asp159. This latter mechanism was suggested for non-heme iron-containing superoxide reductase for which Raman spectroscopy is consistent with a solvent ligand replacing a carboxylate of Glu at the metal accompanied by a blue shift in the visible spectrum from 30 to >100 nm (depending on the enzyme) with only minor changes in the maximal absorption (*54, 55*). These characterized Tyr34 mutants may thus open the door to a variety of experiments aimed at gaining more detailed insight into the MnSOD mechanism. The results and insights presented here furthermore provide a framework for comparative studies on the less studied hexameric NiSOD active site (*56*) as well as on peroxide interactions in the medically important Cu,Zn SOD (*5*) and MnSOD (*21*).

ACKNOWLEDGMENT

We thank the staff of the Advanced Light Source for help in crystallographic data collection.

SUPPORTING INFORMATION AVAILABLE

A figure showing the rate of change of absorbance upon introduction of superoxide to Y34N and Y34F human MnSOD and a figure of extinction coefficients at different wavelengths for Y34A human MnSOD. This material is available free of charge via the Internet at http://pubs.acs.org.

REFERENCES

1. Miller, A. F. (2004) Superoxide dismutases: Active sites that save, but a protein that kills. *Curr. Opin. Chem. Biol. 8*, 162–168.

2. Perry, J. J., Fan, L., and Tainer, J. A. (2007) Developing master keys to brain pathology, cancer and aging from the structural biology of proteins controlling reactive oxygen species and DNA repair. *Neuroscience 145*, 1280–1299.
3. Tainer, J. A., Getzoff, E. D., Beem, K. M., Richardson, J. S., and Richardson, D. C. (1982) Determination and analysis of the 2 Å-structure of copper, zinc superoxide dismutase. *J. Mol. Biol. 160*, 181–217.
4. Tainer, J. A., Getzoff, E. D., Richardson, J. S., and Richardson, D. C. (1983) Structure and mechanism of copper, zinc superoxide dismutase. *Nature 306*, 284–287.
5. Shin, D. S., Didonato, M., Barondeau, D. P., Hura, G. L., Hitomi, C., Berglund, J. A., Getzoff, E. D., Cary, S. C., and Tainer, J. A. (2009) Superoxide dismutase from the eukaryotic thermophile *Alvinella pompejana*: Structures, stability, mechanism, and insights into amyotrophic lateral sclerosis. *J. Mol. Biol. 385*, 1534–1555.
6. Fisher, C. L., Cabelli, D. E., Tainer, J. A., Hallewell, R. A., and Getzoff, E. D. (1994) The role of arginine 143 in the electrostatics and mechanism of Cu,Zn superoxide dismutase: Computational and experimental evaluation by mutational analysis. *Proteins 19*, 24–34.
7. Parge, H. E., Hallewell, R. A., and Tainer, J. A. (1992) Atomic structures of wild-type and thermostable mutant recombinant human Cu,Zn superoxide dismutase. *Proc. Natl. Acad. Sci. U.S.A. 89*, 6109–6113.
8. Bourne, Y., Redford, S. M., Steinman, H. M., Lepock, J. R., Tainer, J. A., and Getzoff, E. D. (1996) Novel dimeric interface and electrostatic recognition in bacterial Cu,Zn superoxide dismutase. *Proc. Natl. Acad. Sci. U.S.A. 93*, 12774–12779.
9. DiDonato, M., Craig, L., Huff, M. E., Thayer, M. M., Cardoso, R. M., Kassmann, C. J., Lo, T. P., Bruns, C. K., Powers, E. T., Kelly, J. W., Getzoff, E. D., and Tainer, J. A. (2003) ALS mutants of human superoxide dismutase form fibrous aggregates via framework destabilization. *J. Mol. Biol. 332*, 601–615.
10. Cardoso, R. M., Thayer, M. M., DiDonato, M., Lo, T. P., Bruns, C. K., Getzoff, E. D., and Tainer, J. A. (2002) Insights into Lou Gehrig's disease from the structure and instability of the A4V mutant of human Cu,Zn superoxide dismutase. *J. Mol. Biol. 324*, 247–256.
11. Deng, H. X., Hentati, A., Tainer, J. A., Iqbal, Z., Cayabyab, A., Hung, W. Y., Getzoff, E. D., Hu, P., Herzfeldt, B., Roos, R. P., et al. (1993) Amyotrophic lateral sclerosis and structural defects in Cu,Zn superoxide dismutase. *Science 261*, 1047–1051.
12. Roberts, B. R., Tainer, J. A., Getzoff, E. D., Malencik, D. A., Anderson, S. R., Bomben, V. C., Meyers, K. R., Karplus, P. A., and Beckman, J. S. (2007) Structural characterization of zinc-deficient human superoxide dismutase and implications for ALS. *J. Mol. Biol. 373*, 877–890.
13. Estevez, A. G., Crow, J. P., Sampson, J. B., Reiter, C., Zhuang, Y., Richardson, G. J., Tarpey, M. M., Barbeito, L., and Beckman, J. S. (1999) Induction of nitric oxide-dependent apoptosis in motor neurons by zinc-deficient superoxide dismutase. *Science 286*, 2498–2500.
14. Borgstahl, G. E., Parge, H. E., Hickey, M. J., Beyer, W. F., Jr., Hallewell, R. A., and Tainer, J. A. (1992) The structure of human mitochondrial manganese superoxide dismutase reveals a novel tetrameric interface of two 4-helix bundles. *Cell 71*, 107–118.
15. Borgstahl, G. E., Parge, H. E., Hickey, M. J., Johnson, M. J., Boissinot, M., Hallewell, R. A., Lepock, J. R., Cabelli, D. E., and Tainer, J. A. (1996) Human mitochondrial manganese superoxide dismutase polymorphic variant Ile58Thr reduces activity by destabilizing the tetrameric interface. *Biochemistry 35*, 4287–4297.
16. Arsova-Sarafinovska, Z., Matevska, N., Petrovski, D., Banev, S., Dzikova, S., Georgiev, V., Sikole, A., Sayal, A., Aydin, A., Suturkova, L., and Dimovski, A. J. (2008) Manganese superoxide dismutase (MnSOD) genetic polymorphism is associated with risk of early-onset prostate cancer. *Cell Biochem. Funct. 26*, 771–777.
17. Nakanishi, S., Yamane, K., Ohishi, W., Nakashima, R., Yoneda, M., Nojima, H., Watanabe, H., and Kohno, N. (2008) Manganese superoxide dismutase Ala16Val polymorphism is associated with the development of type 2 diabetes in Japanese-Americans. *Diabetes Res. Clin. Pract. 81*, 381–385.
18. Bica, C. G., de Moura da Silva, L. L., Toscani, N. V., da Cruz, I. B., Sa, G., Graudenz, M. S., and Zettler, C. G. (2008) MnSOD Gene Polymorphism Association with Steroid-Dependent Cancer. *Pathol. Oncol. Res.* XXX.
19. Kang, D., Lee, K. M., Park, S. K., Berndt, S. I., Peters, U., Reding, D., Chatterjee, N., Welch, R., Chanock, S., Huang, W. Y., and Hayes, R. B. (2007) Functional variant of manganese superoxide dismutase (SOD2 V16A) polymorphism is associated with prostate cancer risk in the prostate, lung, colorectal, and ovarian cancer study. *Cancer Epidemiol., Biomarkers Prev. 16*, 1581–1586.
20. Tugcu, V., Ozbek, E., Aras, B., Arisan, S., Caskurlu, T., and Tasci, A. I. (2007) Manganese superoxide dismutase (Mn-SOD) gene polymorphisms in urolithiasis. *Urol. Res. 35*, 219–224.
21. Li, Y., Huang, T. T., Carlson, E. J., Melov, S., Ursell, P. C., Olson, J. L., Noble, L. J., Yoshimura, M. P., Berger, C., Chan, P. H., Wallace, D. C., and Epstein, C. J. (1995) Dilated cardiomyopathy and neonatal lethality in mutant mice lacking manganese superoxide dismutase. *Nat. Genet. 11*, 376–381.
22. Hallewell, R. A., Laria, I., Tabrizi, A., Carlin, G., Getzoff, E. D., Tainer, J. A., Cousens, L. S., and Mullenbach, G. T. (1989) Genetically engineered polymers of human CuZn superoxide dismutase. Biochemistry and serum half-lives. *J. Biol. Chem. 264*, 5260–5268.
23. Han, W. G., Lovell, T., and Noodleman, L. (2002) Coupled redox potentials in manganese and iron superoxide dismutases from reaction kinetics and density functional/electrostatics calculations. *Inorg. Chem. 41*, 205–218.
24. Miller, A. F., Padmakumar, K., Sorkin, D. L., Karapetian, A., and Vance, C. K. (2003) Proton-coupled electron transfer in Fe-superoxide dismutase and Mn-superoxide dismutase. *J. Inorg. Biochem. 93*, 71–83.
25. Maliekal, J., Karapetian, A., Vance, C., Yikilmaz, E., Wu, Q., Jackson, T., Brunold, T. C., Spiro, T. G., and Miller, A. F. (2002) Comparison and contrasts between the active site PKs of Mn-superoxide dismutase and those of Fe-superoxide dismutase. *J. Am. Chem. Soc. 124*, 15064–15075.
26. Bull, C., Niederhoffer, E. C., Yoshida, T., and Fee, J. A. (1991) Kinetic-Studies of Superoxide Dismutases: Properties of the Manganese-Containing Protein from *Thermus thermophilus*. *J. Am. Chem. Soc. 113*, 4069–4076.
27. Fridovich, I. (1986) Biological effects of the superoxide radical. *Arch. Biochem. Biophys. 247*, 1–11.
28. Jackson, T. A., Karapetian, A., Miller, A. F., and Brunold, T. C. (2005) Probing the geometric and electronic structures of the low-temperature azide adduct and the product-inhibited form of oxidized manganese superoxide dismutase. *Biochemistry 44*, 1504–1520.
29. McAdam, M. E., Fox, R. A., Lavelle, F., and Fielden, E. M. (1977) A pulse-radiolysis study of the manganese-containing superoxide dismutase from *Bacillus stearothermophilus*. A kinetic model for the enzyme action. *Biochem. J. 165*, 71–79.
30. Wintjens, R., Noel, C., May, A. C., Gerbod, D., Dufernez, F., Capron, M., Viscogliosi, E., and Rooman, M. (2004) Specificity and phenetic relationships of iron- and manganese-containing superoxide dismutases on the basis of structure and sequence comparisons. *J. Biol. Chem. 279*, 9248–9254.
31. Ayala, I., Perry, J. J., Szczepanski, J., Tainer, J. A., Vala, M. T., Nick, H. S., and Silverman, D. N. (2005) Hydrogen bonding in human manganese superoxide dismutase containing 3-fluorotyrosine. *Biophys. J. 89*, 4171–4179.
32. Quint, P., Reutzel, R., Mikulski, R., McKenna, R., and Silverman, D. N. (2006) Crystal structure of nitrated human manganese superoxide dismutase: Mechanism of inactivation. *Free Radical Biol. Med. 40*, 453–458.
33. Guan, Y., Hickey, M. J., Borgstahl, G. E., Hallewell, R. A., Lepock, J. R., O'Connor, D., Hsieh, Y., Nick, H. S., Silverman, D. N., and Tainer, J. A. (1998) Crystal structure of Y34F mutant human mitochondrial manganese superoxide dismutase and the functional role of tyrosine 34. *Biochemistry 37*, 4722–4730.
34. Whittaker, M. M., and Whittaker, J. W. (1997) Mutagenesis of a proton linkage pathway in *Escherichia coli* manganese superoxide dismutase. *Biochemistry 36*, 8923–8931.
35. Greenleaf, W. B., Perry, J. J., Hearn, A. S., Cabelli, D. E., Lepock, J. R., Stroupe, M. E., Tainer, J. A., Nick, H. S., and Silverman, D. N. (2004) Role of hydrogen bonding in the active site of human manganese superoxide dismutase. *Biochemistry 43*, 7038–7045.
36. Hearn, A. S., Fan, L., Lepock, J. R., Luba, J. P., Greenleaf, W. B., Cabelli, D. E., Tainer, J. A., Nick, H. S., and Silverman, D. N. (2004) Amino acid substitution at the dimeric interface of human manganese superoxide dismutase. *J. Biol. Chem. 279*, 5861–5866.
37. Edwards, R. A., Whittaker, M. M., Whittaker, J. W., Baker, E. N., and Jameson, G. B. (2001) Outer sphere mutations perturb metal reactivity in manganese superoxide dismutase. *Biochemistry 40*, 15–27.
38. Hsu, J. L., Hsieh, Y., Tu, C., O'Connor, D., Nick, H. S., and Silverman, D. N. (1996) Catalytic properties of human manganese superoxide dismutase. *J. Biol. Chem. 271*, 17687–17691.

39. Ren, X. T., Chingkuang, Bhatt, D., Perry, J. J. P., Tainer, J. A., Cabelli, D. E., and Silverman, D. N. (2005) Kinetic and structural characterization of human manganese superoxide dismutase containing 3-fluorotyrosines. *J. Mol. Struct. 790*, 168–173.
40. Otwinowski, Z., and Minor, W. (1997) Processing of X-ray Diffraction Data Collected in Oscillation Mode. In *Methods in Enzymology* (Carter, C. W., Jr., and Sweet, R. M., Eds.) pp 307−326, Academic Press, New York.
41. McRee, D. E. (1999) XtalView/Xfit: A versatile program for manipulating atomic coordinates and electron density. *J. Struct. Biol. 125*, 156–165.
42. Brunger, A. T., Adams, P. D., Clore, G. M., DeLano, W. L., Gros, P., Grosse-Kunstleve, R. W., Jiang, J. S., Kuszewski, J., Nilges, M., Pannu, N. S., Read, R. J., Rice, L. M., Simonson, T., and Warren, G. L. (1998) Crystallography & NMR system: A new software suite for macromolecular structure determination. *Acta Crystallogr. D54*, 905–921.
43. Sheldrick, G. M. (2008) A short history of SHELX. *Acta Crystallogr. A64*, 112–122.
44. Schwarz, H. A. (1981) Free radicals generated by radiolysis of aqueous solutions. *J. Chem. Educ. 58*, 101–105.
45. Rabani, J., and Nielsen, S. O. (1969) Absorption spectrum and decay kinetics of O_2^- and HO_2 in aqueous solutions by pulse radiolysis. *J. Phys. Chem. 73*, 3736–3744.
46. Hearn, A. S., Stroupe, M. E., Cabelli, D. E., Lepock, J. R., Tainer, J. A., Nick, H. S., and Silverman, D. N. (2001) Kinetic analysis of product inhibition in human manganese superoxide dismutase. *Biochemistry 40*, 12051–12058.
47. Cabelli, D. E., Guan, Y., Leveque, V., Hearn, A. S., Tainer, J. A., Nick, H. S., and Silverman, D. N. (1999) Role of tryptophan 161 in catalysis by human manganese superoxide dismutase. *Biochemistry 38*, 11686–11692.
48. Leveque, V. J., Stroupe, M. E., Lepock, J. R., Cabelli, D. E., Tainer, J. A., Nick, H. S., and Silverman, D. N. (2000) Multiple replacements of glutamine 143 in human manganese superoxide dismutase: Effects on structure, stability, and catalysis. *Biochemistry 39*, 7131–7137.
49. Hsieh, Y., Guan, Y., Tu, C., Bratt, P. J., Angerhofer, A., Lepock, J. R., Hickey, M. J., Tainer, J. A., Nick, H. S., and Silverman, D. N. (1998) Probing the active site of human manganese superoxide dismutase: The role of glutamine 143. *Biochemistry 37*, 4731–4739.
50. Ramilo, C. A., Leveque, V., Guan, Y., Lepock, J. R., Tainer, J. A., Nick, H. S., and Silverman, D. N. (1999) Interrupting the hydrogen bond network at the active site of human manganese superoxide dismutase. *J. Biol. Chem. 274*, 27711–27716.
51. Leveque, V. J., Vance, C. K., Nick, H. S., and Silverman, D. N. (2001) Redox properties of human manganese superoxide dismutase and active-site mutants. *Biochemistry 40*, 10586–10591.
52. Borgstahl, G. E., Pokross, M., Chehab, R., Sekher, A., and Snell, E. H. (2000) Cryo-trapping the six-coordinate, distorted-octahedral active site of manganese superoxide dismutase. *J. Mol. Biol. 296*, 951–959.
53. Lah, M. S., Dixon, M. M., Pattridge, K. A., Stallings, W. C., Fee, J. A., and Ludwig, M. L. (1995) Structure-function in *Escherichia coli* iron superoxide dismutase: Comparisons with the manganese enzyme from *Thermus thermophilus*. *Biochemistry 34*, 1646–1660.
54. Rodrigues, J. V., Abreu, I. A., Cabelli, D., and Teixeira, M. (2006) Superoxide reduction mechanism of *Archaeoglobus fulgidus* one-iron superoxide reductase. *Biochemistry 45*, 9266–9278.
55. Mathe, C., Niviere, V., and Mattioli, T. A. (2005) Fe^{3+}-hydroxide ligation in the superoxide reductase from *Desulfoarculus baarsii* is associated with pH dependent spectral changes. *J. Am. Chem. Soc. 127*, 16436–16441.
56. Barondeau, D. P., Kassmann, C. J., Bruns, C. K., Tainer, J. A., and Getzoff, E. D. (2004) Nickel superoxide dismutase structure and mechanism. *Biochemistry 43*, 8038–8047.

BI8023288